Quantum rainbow channeling of positrons in very short carbon nanotubes

S. Petrović,* M. Ćosić, and N. Nešković
Laboratory of Physics, Vinča Institute of Nuclear Sciences, University of Belgrade, P.O. Box 522, 11001 Belgrade, Serbia
(Received 1 March 2013; published 12 July 2013)

This is a theoretical study of transmission of positrons of kinetic energies of 1 and 10 MeV through very short (11,9) single-wall carbon nanotubes of lengths of 200 and 560 nm, respectively. The needed continuum interaction potential of the positron and nanotube is obtained starting from the Molière's approximation of the Thomas-Fermi interaction potential of a positron and a nanotube atom. We calculate the classical and quantum angular distributions of transmitted positrons. In the classical calculations, the approach is via the equations of motion, and in the quantum calculations, the time-dependent Schrödinger equation is solved. The solutions of these equations are obtained numerically. In the quantum calculations, the initial beam is taken to be an ensemble of noninteracting Gaussian wave packets. The angular distributions are generated using the computer simulation method. Our analysis is concentrated on the rainbow effect, which is clearly seen in the angular distributions. The obtained classical and quantum rainbows are analyzed in detail and compared with each other.

DOI: 10.1103/PhysRevA.88.012902 PACS number(s): 61.85.+p

I. INTRODUCTION

The channeling of a charged particle in a crystal is its motion through the axial or planar crystal channels [1–3]. In this process, the angle between the particle momentum vector and the channel axis or the median plane remains small. When the rainbow lines appear in the transmission angle plane, determining the angular distribution of transmitted particles, the process is called rainbow channeling [4–7]. When, in addition, the values of the particle mass and the kinetic energy are such that the channeled particles exhibit their wave properties, the process is called quantum rainbow channeling.

Andersen *et al.* [8] registered the quantum behavior of positrons of kinetic energy of 1 MeV that were channeled in a gold crystal and then backscattered from it. A similar experiment with the same result was performed with 1.2-MeV positrons and a silicon crystal by Pedersen *et al.* [9]. In both measurements, the positrons moved along the planar crystal channels. Haakenaasen *et al.* [10] observed the pronounced quantum behavior of 1-MeV positrons transmitted through the axial as well as the planar channels of a silicon crystal. All those measurements were analyzed using the dynamical diffraction theory, which is based on the expansion of the positron wave function in Bloch wave functions [11].

Carbon nanotubes were discovered by Iijima [12]. One can describe them as sheets of carbon atoms rolled up into cylinders with the atoms lying at the hexagonal crystal lattice sites. The nanotube diameters are of the order of a nanometer and their lengths can be more than 100 μm. Nanotubes can be single-wall or multiwall structures, depending on the number of cylinders they include. They have remarkable physical properties [13]. As a result, they have begun to play an important role in the field of nanotechnology [14]. A nanotube is achiral or chiral. In the former case, it is composed of atomic strings parallel to its axis, and in the latter case, it consists of atomic strings that spiral around the axis.

Soon after the discovery of carbon nanotubes, Klimov and Letokhov [15] predicted that they could be used to channel positively charged particles. After that, a number of theoretical groups studied ion channeling in nanotubes. A list of their most important publications is given in Ref. [16]. The main objective of most of those studies was to investigate the possibility of guiding ion beams with nantoubes. The experimental study of ion channeling in nanotubes is still in the initial phase [17,18].

It is well known that the rainbow effect occurs when sunlight scatters from water droplets [19,20]. The study of it began in ancient times. Such an effect also occurs and plays an important role in nucleus-nucleus collisions [21,22], atom or ion collisions with atoms or molecules [23], electron-molecule collisions [24], atom, ion, or electron scattering from crystal surfaces [25–28], and ion channeling in crystals [4–7].

Besides, Petrović *et al.* [29] showed that the rainbow effect could also occur in ion channeling in carbon nanotubes. They demonstrated that the theory of crystal rainbows [6] provided the full explanation of the obtained angular distributions of transmitted ions. In that study, the projectiles were 1-GeV protons and the target was a 1-μm-long bundle of (10,10) single-wall carbon nanotubes (SWCNs). Those nanotubes were very short. The same group has also explored the rainbow effect in proton channeling in short and long (11,9) SWCNs [30,31].

Here, we present a study of the transmission of 1- and 10-MeV positrons through very short (11,9) SWCNs. It includes classical and quantum calculations and is concentrated on the rainbow effect.

II. THEORETICAL FRAMEWORK

The system we consider is a positron channeled in a (11,9) SWCN. As it has been said above, the values of positron kinetic energy are $E = 1$ and 10 MeV. In the former case, the value of the nanotube length is $L = 200$ nm. The corresponding value of the reduced nanotube length is $\Lambda = 0.12$. In the latter case, $L = 560$ nm. This value has been chosen to obtain the same value of Λ as in the former case (0.12). The reduced nanotube length is defined as

$$\Lambda = f_h \frac{mL}{p_0}, \tag{1}$$

*Corresponding author: petrovs@vinca.rs

where m is the positron relativistic mass, p_0 is the magnitude of initial positron momentum vector, and f_h is the frequency of positron motion close to the nanotube axis [5]. The fact that the value of Λ in question is below 0.25 means that both nanotubes are very short [6]. We take that the z axis of the reference frame, being the longitudinal axis, coincides with the nanotube axis and that its origin lies in the nanotube entrance plane. The x and y axes, being the transverse axes, are the vertical and horizontal axes, respectively.

A. Interaction potentials

In this study, the interaction of the positron and a nanotube atom is described by Moliere's approximation of the Thomas-Fermi interaction potential [32]. The needed continuum interaction potential of the positron and nanotube is obtained in three steps. The first step is the axial averaging of the positron-atom interaction potential, on the basis of the continuum approximation [2]. It should be mentioned here that the use of this approximation for very thin crystals has been recently justified in a high-resolution channeling experiment with 2-MeV protons and a 55-nm-thick ⟨100⟩ silicon crystal [7]. The second step is the azimuthal averaging of the interaction potential obtained in the first step, on the basis of the fact that the nanotube is chiral. The resulting continuum positron-nanotube interaction potential reads

$$U(\rho; R_n) = U_0 \sum_{i=1}^{3} \alpha_i K_0\left(\frac{\beta_i R_n}{a_s}\right) I_0\left(\frac{\beta_i \rho}{a_s}\right) \quad \text{for} \quad \rho \leqslant R_n, \tag{2}$$

and

$$U(\rho; R_n) = U_0 \sum_{i=1}^{3} \alpha_i I_0\left(\frac{\beta_i R_n}{a_s}\right) K_0\left(\frac{\beta_i \rho}{a_s}\right) \quad \text{for} \quad \rho > R_n, \tag{3}$$

with

$$U_0 = \frac{16\pi Z_2 e^2 R_n}{3^{4/3} a_b^2}, \tag{4}$$

where Z_2 is the nanotube atom atomic number, e is the elementary charge, $\rho = (x^2 + y^2)^{1/2}$, x and y are the transverse components of positron position vector, $a_s = [9\pi^2/(128 Z_2)]^{1/3} a_0 = 0.026$ nm is the nanotube atom screening radius [33], a_0 is the Bohr radius, a_b is the nanotube atoms bond length [13], $R_n = 0.69$ nm is the equilibrium nanotube radius [13], $(\alpha_i) = (0.35, 0.55, 0.10)$ and $(\beta_i) = (0.1, 1.2, 6.0)$ are the fitting parameters, and I_0 and K_0 designate the modified Bessel functions of the first and second kinds and 0th order, respectively [34]. This function is continuous but its first derivative is discontinuous at point $\rho = R_n$.

In the third step, the thermal vibrations of the nanotube atoms are introduced. This is done by the initial averaging of the interaction potential of the positron and a nanotube atom over its displacements from the equilibrium position along the x, y, and z axes [35]. These displacements are taken to be small and independent and are described by a Gaussian distribution function. This averaging appears in the third step as the averaging of the interaction potential obtained in the second step over the effective thermally induced changes of the nanotube radius, R, from its equilibrium radius, R_n, along the ρ axis. The resulting continuum positron-nanotube interaction potential is given by

$$U_{\rm qu}^{\rm th}(\rho; R_n) = \frac{1}{(2\pi)^{1/2}\sigma_{\rm th}} \int_{R_1}^{R_2} U(\rho; R) \exp\left[-\frac{(R - R_n)^2}{2\sigma_{\rm th}^2}\right] dR, \tag{5}$$

where $\sigma_{\rm th} = 0.0053$ nm [36] is the one-dimensional thermal vibration amplitude of the nanotube atoms. The integration limits appearing in this expression are $R_1 = R_n - 6\sigma_{\rm th}$ and $R_2 = R_n + 6\sigma_{\rm th}$. They have been chosen to comprise the interval in which the changes of the integrand are not negligible. The integration is performed numerically. This function and its first derivative are continuous; i.e., its first derivative is not discontinuous at point $\rho = R_n$. However, since the displacements of the nanotube atoms are small, a useful analytical approximation of Eq. (5) can be obtained by substituting $U(\rho, R)$, represented as a function of $\rho - R$, with its Tailor series about point $\rho - R_n$ truncated after its second order term [31]. For $\rho \leqslant R_n$, this expression becomes

$$U_{\rm cl}^{\rm th}(\rho; R_n) = U_0 \sum_{i=1}^{3} \left(\alpha_i + \frac{\sigma_{\rm th}^2 \beta_i^2}{2a_s^2}\right) K_0\left(\frac{\beta_i R_n}{a_s}\right) I_0\left(\frac{\beta_i \rho}{a_s}\right). \tag{6}$$

This function is continuous but its first derivative is discontinuous at point $\rho = R_n$, in a way similar to that of $U(\rho; R_n)$, given by Eqs. (2) and (4). The analysis has shown that the difference between $U_{\rm cl}^{\rm th}(\rho; R_n)$ and $U_{\rm qu}^{\rm th}(\rho; R_n)$ is very small, especially for $\rho \leqslant R_n - a_s$.

In the classical calculations to be presented here, we have used $U_{\rm cl}^{\rm th}(\rho; R_n)$, given by Eqs. (6) and (4), as the needed continuum positron-nanotube interaction potential. This has been done because in these calculations $\rho \leqslant R_n - a_s$. On the other hand, the quantum calculations have been performed with $U_{\rm qu}^{\rm th}(\rho; R_n)$, given by Eqs. (6) and (2)–(4), as the needed continuum positron-nanotube interaction potential. The reason is the fact that the discontinuity of function $U_{\rm cl}^{\rm th}(\rho; R_n)$ at point $\rho = R_n$, which must not be excluded from these calculations, has proven to be a source of serious numerical problems. It is important to note that the functions $U_{\rm cl}^{\rm th}(\rho; R_n)$ and $U_{\rm qu}^{\rm th}(\rho; R_n)$ are cylindrically symmetric.

B. Classical approach

Let us designate the vertical and horizontal components of the initial positron position vector, in the entrance plane of the nanotube, as the components of its impact parameter vector (in the impact parameter plane), by x_0 and y_0, and the vertical and horizontal components of its initial momentum vectors by p_{x_0} and p_{y_0}, respectively. The vertical and horizontal components of the final positron position vector, in the exit plane of the nanotube, are designated by x and y, and the vertical and horizontal components of its final momentum vector by p_x and p_y, respectively. In the classical calculations to be described here, the approach is via the equations of motion. As a consequence of the axial averaging of the positron-atom interaction potential, x, y, p_x, and p_y are obtained by solving the positron equations of motion in the transverse position

plane, which read

$$m\frac{d^2x}{dt^2} = -\partial_x U_{\rm cl}^{\rm th}(\rho; R_n) \quad \text{and} \quad m\frac{d^2y}{dt^2} = -\partial_y U_{\rm cl}^{\rm th}(\rho; R_n), \tag{7}$$

where $\partial_x = \partial/\partial_x$, $\partial_y = \partial/\partial y$, and t denotes time. They are solved numerically by the Runge-Kutta method of the fourth order [37]. Since the nanotube is very short, the positron energy loss and dispersion of its channeling angle, which are caused by its collisions with the nanotube electrons, are neglected. As it has been said above, during the channeling process, the angle between the positron momentum vector and the nanotube axis remains small. The corresponding critical angle is

$$\theta_c = \left[\frac{U_{\rm cl}^{\rm th}(R_n - a_s; R_n)}{E}\right]^{1/2}. \tag{8}$$

For $E = 1$ MeV, $\theta_c = 7.3$ mrad, while for $E = 10$ MeV, $\theta_c = 2.3$ mrad. Therefore, the vertical and horizontal components of the positron transmission angle (in the transmission angle plane) are $\theta_x = p_x/p$ and $\theta_y = p_y/p$, respectively, where $p = p_0$ is the magnitude of final positron momentum vector. The initial values of θ_x and θ_y are $\theta_{x_0} = p_{x_0}/p$ and $\theta_{y_0} = p_{y_0}/p$, respectively.

Since the interaction of the positron and nanotube is cylindrically symmetric, the mapping of the impact parameter plane to the final transverse position plane or to the transmission angle plane is reduced to the mapping of, e.g., the x_0 axis in the impact parameter plane to the x axis in the final transverse position plane or to the θ_x axis in the transmission angle plane. We shall refer to the former mapping, $x(x_0)$, as the spatial transmission function and to the latter mapping, $\theta_x(x_0)$, as the angular transmission function of the positron through the nanotube.

The spatial and angular distributions of transmitted positrons, i.e., their distributions in the final transverse position plane and transmission angle plane, respectively, are generated using the computer simulation method. The pairs of values of x_0 and y_0 are chosen randomly within region $\rho \leqslant R_n - a_s$. The chosen limiting value of ρ ensures that large values of the transmission angle are avoided. It is assumed that the initial positron beam diverges from the nanotube axis. Its full-width-at-half-maximum (FWHM) is designated by Δ_d. The values of θ_{x_0} and θ_{y_0} are chosen via the Gaussian distribution functions with the corresponding standard deviation being $\sigma_\theta = \Delta_d/(8\ln 2)^{1/2}$.

C. Quantum mechanical approach

In the quantum calculations within this study, the approach is via the time-dependent Schrödinger equation. As a consequence of the axial averaging of the positron-atom interaction potential, we solve the time-dependent positron Schrödinger equation in the transverse position plane, which reads

$$i\hbar\partial_t \psi_s(x,y,t) = -\frac{\hbar^2}{2m}\Delta\psi_s(x,y,t) + U_{\rm qu}^{\rm th}(\rho; R_n)\psi_s(x,y,t), \tag{9}$$

where $\psi_s(x,y,t)$ is the positron wave function in the transverse position plane, $\Delta = \partial^2/\partial x^2 + \partial^2/\partial y^2$, $\partial_t = \partial/\partial_t$, and $\hbar$ is the reduced Planck constant.

In this study, the initial positron beam is taken to be an ensemble of noninteracting Gaussian wave packets. It should be emphasized that this is a novel approach—we are not aware of a similar treatment of particle channeling in crystals or nanotubes thus far. In this approach, the divergence of the initial beam from the nanotube axis is taken into account implicitly. In the coordinate representation, an initial wave packet, for $t = 0$, is described by the function

$$\psi_s(x,y,0; x_0, y_0) = \frac{1}{(2\pi)^{1/2}\sigma_\rho} \times \exp\left[-\frac{(x-x_0)^2 + (y-y_0)^2}{4\sigma_\rho^2}\right], \tag{10}$$

where σ_ρ is its spatial standard deviation. In the momentum representation, the initial wave packet is described by the function

$$\psi_a(\theta_x,\theta_y; x_0, y_0) = \frac{1}{(2\pi)^{1/2}\sigma_\theta}\exp\left[-\frac{ip(x_0\theta_x + y_0\theta_y)}{\hbar}\right] \times \exp\left[-\frac{\theta_x^2 + \theta_y^2}{4\sigma_\theta^2}\right], \tag{11}$$

which is obtained via the Fourier transformation of Eq. (10), where $\sigma_\theta = \Delta_d/(8\ln 2)^{1/2}$ is its angular standard deviation, with Δ_d being the initial beam FWHM. Parameters σ_ρ and σ_θ are connected to each other by the expression $\sigma_\rho\sigma_\theta = \hbar/(2p)$, representing the uncertainty principle in the problem under consideration.

In the coordinate representation, the final wave packet is described by the function $\psi_s(x,y,t;\, x_0,y_0)$ obtained as the solution of Eq. (9) for $t = mL/p$. The equation is solved numerically using the Chebishev global propagation method [38]. The computation domain is region $-D_x/2 \leqslant x \leqslant D_x/2$ and region $-D_y/2 \leqslant y \leqslant D_y/2$, with $D_x = D_y = 3R_n$. It has been established that, in order to avoid problems in applying this method, the needed continuum positron-nanotube interaction potential and its first derivative must be continuous in the whole transverse position plane, including point $\rho = R_n$. That is why we use Eq. (5) in the quantum calculations. The spatial distribution of transmitted positrons is given as a weighted sum of the final positron spatial probability functions over the chosen values of x_0 and y_0,

$$Y_s(x,y) = \sum_{x_0,y_0} c(x_0,y_0)|\psi_s(x,y,t;x_0,y_0)|^2. \tag{12}$$

The pairs of values of x_0 and y_0 are chosen within region $\rho \leqslant R_n - a_s$. This should be done randomly and the number of the pairs of values should be large. In that case, each of the coefficients $c(x_0,y_0)$ would be equal to $1/N$, with N being the initial number of positrons. However, in order to minimize the computation time, the pairs of values of x_0 and y_0 are chosen using an algorithm providing a minimal deviation of the initial spatial distribution of positrons from the uniform distribution within region $\rho \leqslant R_n - a_s$ with a smaller number of pairs. This uniform distribution is given by $1/[\pi(R_n - a_s)^2]$. We achieve this by adjusting the values of $c(x_0,y_0)$.

In the momentum representation, the final wave packet is described by the function $\psi_s(\theta_x,\theta_y,t;\, x_0,y_0)$, obtained via

the Fourier transformation of $\psi_s(x,y,t;x_0,y_0)$ for $t = mL/p$. The transformation is performed numerically. The angular distribution of transmitted positrons is given as the weighted sum of the final positron angular probability functions over the chosen values of x_0 and y_0,

$$Y_a(\theta_x,\theta_y) = \sum_{x_0,y_0} c(x_0,y_0)|\psi_a(\theta_x,\theta_y,t,x_0,y_0)|^2. \quad (13)$$

We also analyze here the case in which the initial positron beam is represented as the plane wave. In this case, in the coordinate representation, the initial beam spatial probability function is derived from Eq. (10) with the condition $\sigma_\rho \to \infty$. It reads $1/(2\pi\sigma_\rho^2)$. In the momentum representation, the initial beam angular probability function is derived from Eq. (11) with the condition $\sigma_\theta \to 0$. It reads $\delta(\theta_x)\delta(\theta_y)$, where δ designates the Dirac δ function. However, this means that the solving of Eq. (9) would have to begin with a function having a very small constant value in the whole computation domain. That would be a source of serious numerical problems. Therefore, we choose for the initial wave function in the coordinate representation the function having the constant value in the whole computation domain that is determined by the appropriate normalization condition,

$$\psi_s(x,y,0) = \frac{1}{(D_x D_y)^{1/2}}. \quad (14)$$

This value has proven to be sufficiently large to avoid numerical problems. The corresponding initial wave function in the momentum representation is obtained numerically via the Fourier transformation of Eq. (14). It is different from zero only at the origin and the corresponding value is

$$\psi_a(\theta_x,\theta_y,0) = \frac{p(D_x D_y)^{1/2}}{2\pi\hbar}. \quad (15)$$

As it has been already said, in the coordinate representation, the final wave function, $\psi_s(x,y,t)$, is obtained as the solution of Eq. (9) for with $t = mL/p$. Again, the equation is solved numerically using the Chebishev global propagation method [38]. The spatial distribution of the transmitted positrons is

$$Y_s(x,y) = |\psi_s(x,y,t)|^2. \quad (16)$$

In the momentum representation, the final wave function, $\psi_a(\theta_x,\theta_y,t)$, is obtained via the Fourier transformation of $\psi_s(x,y,t)$ for $t = mL/p$. The transformation is performed numerically. The angular distribution of the transmitted positrons is

$$Y_a(\theta_x,\theta_y) = |\psi_a(\theta_x,\theta_y,t)|^2. \quad (17)$$

III. RESULTS AND DISCUSSION

A. Classical calculations

Figure 1(a) shows the spatial transmission function of 1-MeV positrons through a 200-nm-long (11,9) SWCN for the initial positron momentum vector parallel to the nanotube axis. This function has two pairs of extrema—a maximum and minimum designated by $1^{s,1}$, and a miminum and maximum designated by $2^{s,1}$. Extrema $1^{s,1}$ lie at points $x_{01}^{s,1} = 0.29$ nm and extrema $2^{s,1}$ at points $x_{02}^{s,1} = \pm 0.64$ nm. This means

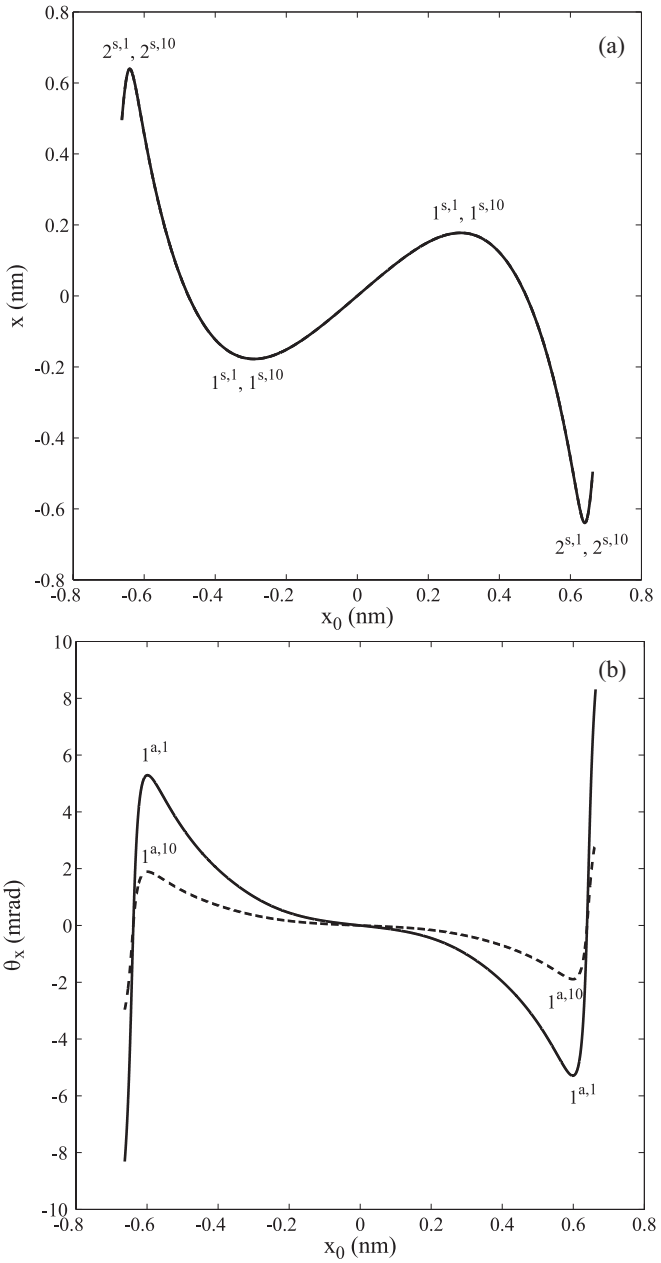

FIG. 1. (a) Spatial transmission functions of 1-MeV positrons through a 200-nm-long (11,9) SWCN (solid line) and of 10-MeV positrons through a 560-nm-long (11,9) SWCN (dashed line, coinciding with the solid line) for $p_{x0} = 0$ and $p_{y0} = 0$. (b) The corresponding angular transmission functions, which do not coincide.

that there are two circular spatial rainbow lines in the impact parameter plane, whose radii are $|x_{01}^{s,1}|$ and $|x_{02}^{s,1}|$. The corresponding values of the spatial transmission function are $x_1^{s,1} = \pm 0.18$ and $x_2^{s,1} = \pm 0.64$ nm, respectively. Thus, there are two circular rainbow lines in the final transverse position plane, being the images of the spatial rainbow lines in the impact parameter plane, whose radii are $|x_1^{s,1}|$ and $|x_2^{s,1}|$. The analysis has shown that the positron trajectories corresponding to extrema $1^{s,1}$ involve one deflection from the nanotube wall and the trajectories corresponding to extrema $2^{s,1}$ two deflections from the nanotube wall. Hence, one can

say that the former extrema belong to a primary rainbow and the latter extrema to a secondary rainbow in the final transverse position plane.

It is evident that the inverse function of this spatial transmission function has five branches, which are separated by the rainbow extrema. It is triple valued in the region between -0.18 and $+0.18$ nm, single valued in the regions between -0.50 and -0.18 nm and between $+0.18$ and $+0.50$ nm, and double valued in the regions between -0.64 and -0.50 nm and between $+0.50$ and $+0.64$ nm. Therefore, the inner side of each of the two rainbow lines in the final transverse position plane is recognized as the bright side of the rainbow and its outer side as the dark side of the rainbow.

Figure 1(a) also gives the spatial transmission function of 10-MeV positrons through a 560-nm-long (11,9) SWCN with the initial positron momentum vector parallel to the nanotube axis. It coincides with the corresponding spatial transmission functions in the case of $E = 1$ MeV. This is a consequence of the fact that, in these two cases, the values of Λ coincide. The primary and secondary rainbow extrema that occur in the case of $E = 10$ MeV are designated by $1^{s,10}$ and $2^{s,10}$, the points at which they lie by $x_{01}^{s,10}$ and $x_{02}^{s,10}$, and the corresponding values of spatial transmission function by $x_1^{s,10}$ and $x_2^{s,10}$, respectively.

Figure 1(b) shows the angular transmission function of 1-MeV positrons through a 200-nm-long (11,9) SWCN with the initial positron momentum vector parallel to the nanotube axis. This function has a pair of extrema—a minimum and maximum designated by $1^{a,1}$. They lie at points $x_{01}^{a,1} = \pm 0.60$ nm. This means that there is one circular angular rainbow line in the impact parameter plane, whose radius is $|x_{01}^{a,1}|$. The corresponding values of the angular transmission function are $\theta_{x1}^{a,1} = \pm 5.3$ mrad. Hence, there is one circular rainbow line in the transmission angle plane, being the image of the angular rainbow line in the impact parameter plane, whose radius is $|\theta_{x1}^{a,1}|$. It has been found that the positron trajectories corresponding to extrema $1^{a,1}$ involve one deflection from the nanotube wall. Thus, one can conclude that these extrema belong to a primary rainbow in the transmission angle plane.

It is evident that the inverse function of this angular transmission function has three branches. It is triple valued in the region between -5.3 and $+5.3$ mrad and single valued in the regions between -8.3 and -5.3 mrad and between $+5.3$ and $+8.3$ mrad. Therefore, the inner side of the rainbow line in the transmission angle plane is recognized as the bright side of the rainbow and its outer side as the dark side of the rainbow.

Figure 1(b) also gives the angular transmission function of 10-MeV positrons through a 560-nm-long (11,9) SWCN with the initial positron momentum vector parallel to the nanotube axis. As the corresponding angular transmission function in the case of $E = 1$ MeV, this function has a minimum and maximum lying at points $x_{01}^{a,10} = \pm 0.60$ nm. However, the corresponding values of the angular transmission function are $\theta_{x1}^{a,10} = \pm 1.9$ mrad. These extrema, designated by $1^{a,10}$, belong to a primary rainbow in the transmission angle plane.

Figure 2 gives the angular transmission function of 1-MeV positrons through a 200-nm-long (11,9) SWCN as a function of the corresponding spatial transmission function with the initial positron momentum vector parallel to the nanotube axis. We refer to the diagram representing this dependence as the rainbow diagram of the positrons transmitted through the nanotube. The tangents of this diagram perpendicular to the x axis determine the positions of the four rainbow extrema in the final transverse position plane while its tangents perpendicular to the θ_x axis determine the positions of the two rainbow extrema in the transmission angle plane. This figure also gives the corresponding rainbow diagram in the case of $E = 10$ MeV.

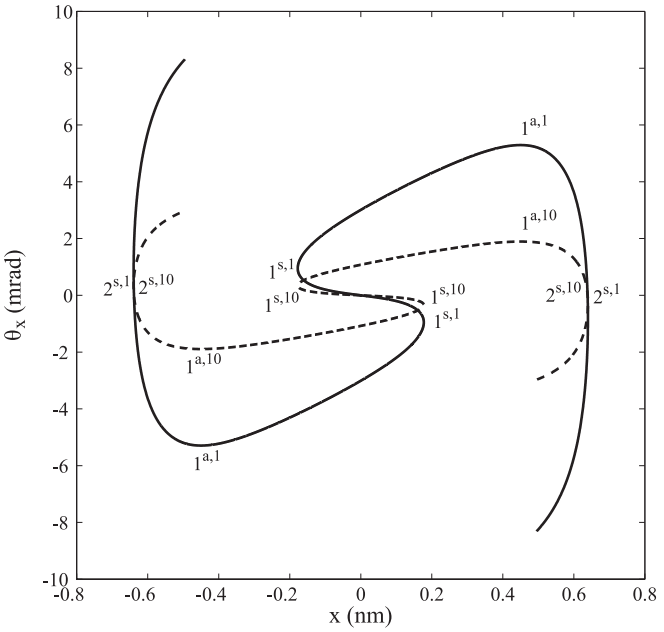

FIG. 2. Rainbow diagrams of 1-MeV positrons transmitted through a 200-nm-long (11,9) SWCN (solid line) and of 10-MeV positrons transmitted through a 560-nm-long (11,9) SWCN (dashed line) for $p_{x0} = 0$ and $p_{y0} = 0$.

Figure 3 gives the normalized classical distribution along the θ_x axis of 1-MeV positrons transmitted through a 200-nm-long (11,9) SWCN with the initial beam parallel to the nanotube axis. The initial number of positrons is $N = 1 \times 10^8$. It has a strong maximum corresponding to the nanotube axis and a pair of weak maxima lying at points $\theta_{x1}^{a,1}$. A comparison of this figure with Fig. 1(b) shows that the weak maxima are the classical primary rainbow maxima. They are designated by 1_{cl}. The fact that the distribution contains the positrons with the transmission angles beyond the rainbow maxima, i.e., below -5.3 mrad and above $+5.3$ mrad, is attributed to the fact that a branch of the angular transmission function exists in each of these regions. This figure also shows the normalized classical angular distribution of 1-MeV positrons transmitted through a 200-nm-long (11,9) SWCN with the initial beam diverging from the nanotube axis and having Δ_d that gives $\sigma_\theta = 0.1\theta_c = 0.73$ mrad. Again, the initial number of positrons is $N = 1 \times 10^8$. In this case, the classical primary rainbow maxima, designated by $1_{\mathrm{cl}}'$, lie at points ± 5.1 mrad. One can say that the divergence of the initial beam caused the rainbow maxima to move slightly toward the origin and lose some strength.

It should be mentioned here that the angular distribution of the transmitted positrons does not coincide with their spatial distribution that would be measured with a detector placed

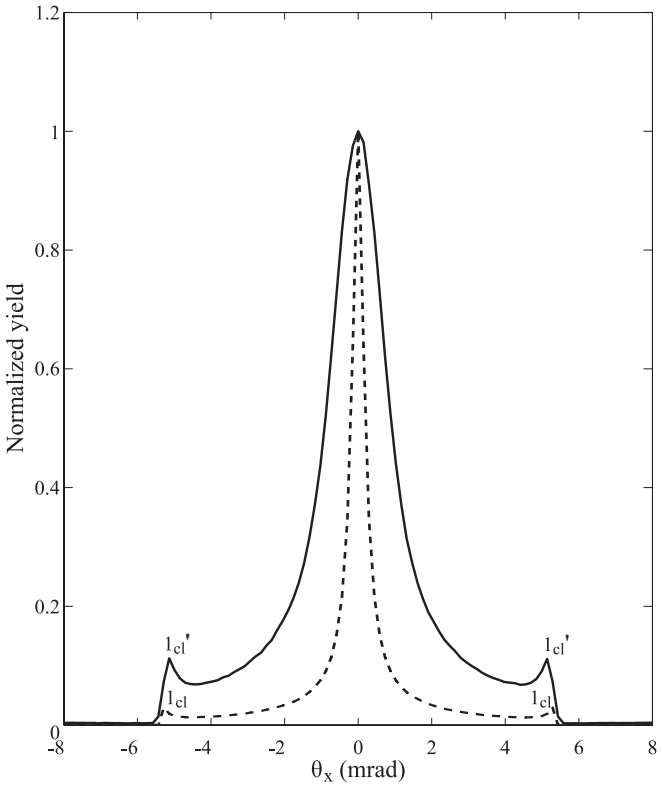

FIG. 3. One-dimensional normalized classical angular distributions of 1-MeV positrons transmitted through a 200-nm-long (11,9) SWCN for $\sigma_\theta = 0$ (dashed line) and $\sigma_\theta = 0.1\theta_c$ (solid line).

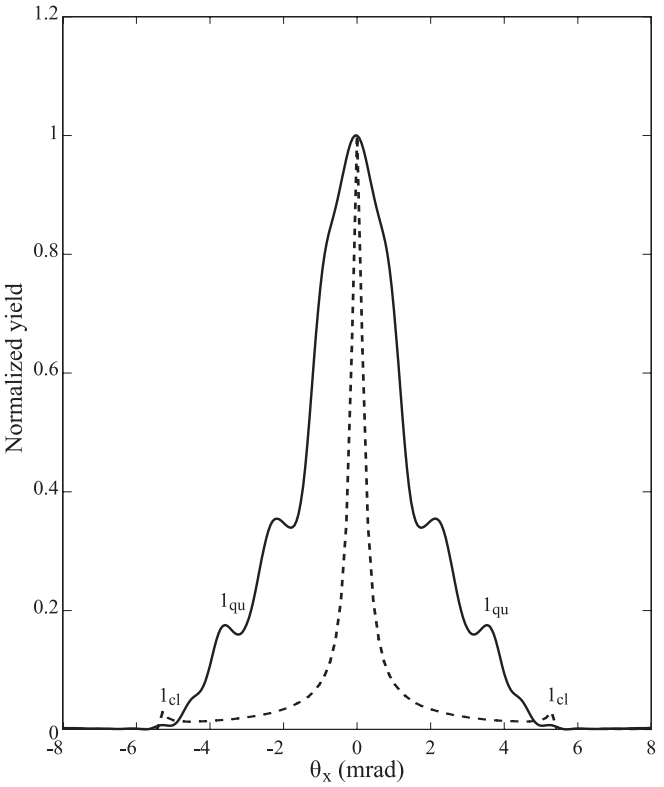

FIG. 4. One-dimensional normalized angular distribution of 1-MeV positrons transmitted through a 200-nm-long (11,9) SWCN with the initial beam represented as the plane wave (solid line) and the corresponding classical angular distribution, for $\sigma_\theta = 0$ (dashed line).

close to the nanotube exit. However, if the detector were placed far away from the nanotube exit, it would give the spatial distribution that coincides with the angular distribution with the scaled abscissa. The scaling factor is the distance of the detector from the nanotube exit.

B. Quantum mechanical calculations

Figure 4 shows the normalized angular distribution of 1-MeV positrons transmitted through a 200-nm-long (11,9) SWCN with the initial beam represented as the plane wave together with the corresponding classical distribution, with the initial beam parallel to the nanotube axis (see Fig. 3). The quantum distribution can be viewed as the superposition of a bell-shaped component and a component consisting of five pairs of maxima. Among these pairs of maxima, the ones laying at points ± 3.5 and ± 2.2 mrad are more pronounced than the others. We explain these maxima by the fact that the inverse function of the corresponding angular transmission function is triple valued on the bright side of the classical primary rainbow [see Fig. 1(b)]. They appear due to the constructive interference of the three rays within the plane wave that have the same position in the transmission angle plane [19–21]. These rays interfere since their path lengths through the nanotube and, hence, the phases they accumulate during the transmission, are different.

Figures 5(a) and 5(b) give the two-dimensional initial spatial and angular distributions of a 1-MeV positron represented as the Gaussian wave packet with the angular standard deviation $\sigma_\theta = 0.1\theta_c = 0.73$ mrad, giving the spatial standard deviation $\sigma_\rho = 0.19$ nm, which is placed at the intersection of the primary angular rainbow line in the impact parameter plane and the x axis, respectively. The resulting spatial and angular distributions of the positron transmitted through a 200-nm-long (11,9) SWCN are given in Figs. 5(c) and 5(d), respectively. One can see that the resulting spatial distribution contains a strong maximum and a number of additional weaker maxima extending from the nanotube wall toward its axis and beyond it. We explain these maxima by the fact that the inverse function of the corresponding spatial transmission function is double valued in the vicinity of the classical secondary rainbow and that the initial wave packet covers the two branches of the inverse function [see Fig. 1(a)]. They appear due to the constructive interference of the two rays within the wave packet that have the same position in the final transverse position plane [19–21]. The resulting angular distribution contains a strong maximum and several weaker maxima extending toward the origin and beyond it. Similarly, these maxima are explained by the fact that the inverse function of the corresponding angular transmission function is double valued in the vicinity of the classical primary rainbow and that the initial wave packet covers the two branches of the inverse function [see Fig. 1(b)]. They appear due to the constructive interference of the two rays within the wave packet that have the same position in the transmission angle plane [19–21].

Figure 6 shows the one-dimensional angular distributions of the transmitted positrons for $E = 1$ MeV and $L = 200$ nm with the positrons represented initially as the Gaussian wave packets

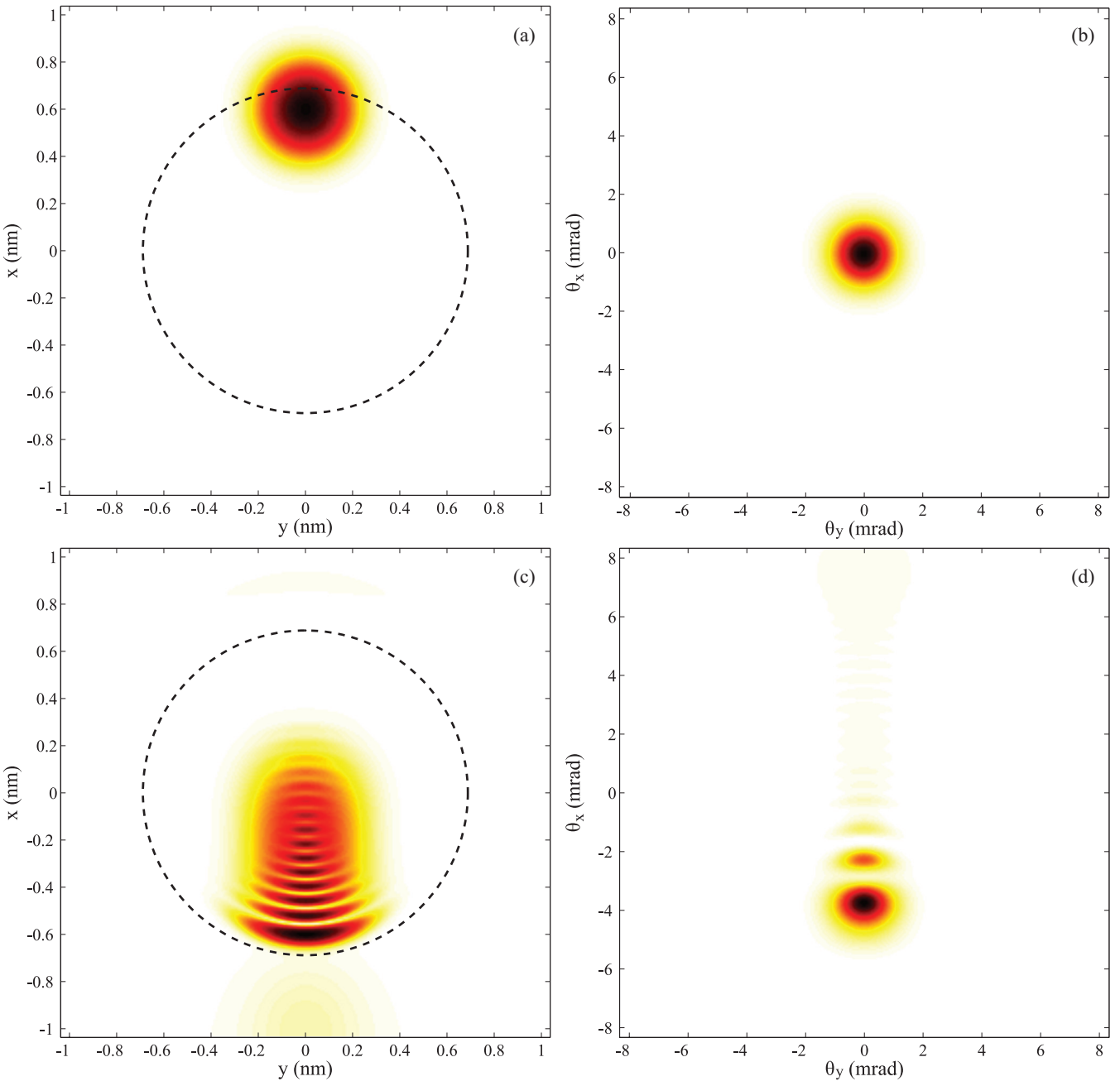

FIG. 5. (Color online) (a) Two-dimensional initial spatial distribution of a 1-MeV positron represented as the Gaussian wave packet with $\sigma_\theta = 0.1\theta_c$ and $(x_0, y_0) = (0.599\ \text{nm}, 0)$, (b) the corresponding initial angular distribution, (c) the resulting spatial distribution of the positron transmitted through a 200-nm-long (11,9) SWCN, and (d) the corresponding resulting angular distribution. The dashed circle, appearing in panels (a) and (c), represents the nanotube wall.

with $\sigma_\theta = 0.1\theta_c = 0.73$ mrad, giving $\sigma_\rho = 0.19$ nm, placed at the intersection of the primary angular rainbow line in the impact parameter plane and the x axis, close to this intersection toward the nanotube axis, and at the axis. The first distribution is contained in the two-dimensional angular distribution shown in Fig. 5(d). The strongest maximum lies at point -3.8 mrad and the next two weaker maxima lie at points -2.3 and -1.2 mrad. On the basis of the above given explanation, one can state that the strongest maximum of the distribution belongs to the quantum primary rainbow and the two weaker maxima belong to the first and second primary supernumerary rainbows [19–21]. The second distribution is similar to the first distribution. This can be explained by the fact that the corresponding initial wave packet is placed sufficiently close to the primary angular rainbow line in the impact parameter plane to cover the two branches of the transmission function. The third distribution is a bell-shaped one with no maxima that would be attributed to the interference of rays within the wave packet. This is understandable since the corresponding initial wave packet is placed sufficiently far away from the primary angular rainbow line in the impact parameter plane and, therefore, covers only one branch of the transmission function.

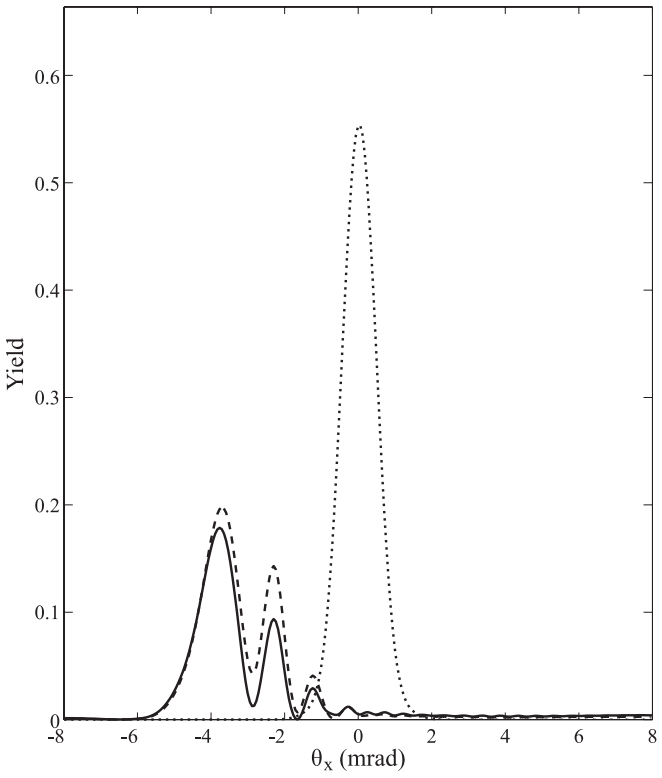

FIG. 6. One-dimensional angular distributions of 1-MeV positrons transmitted through a 200-nm-long (11,9) SWCN with the positrons represented initially as the Gaussian wave packets with $\sigma_\theta = 0.1\theta_c$ and $(x_0, y_0) = (0,0)$ (dotted line), $(x_0, y_0) = (0.552\text{ nm}, 0)$ (dashed line), and $(x_0, y_0) = (0.599\text{ nm}, 0)$ (solid line).

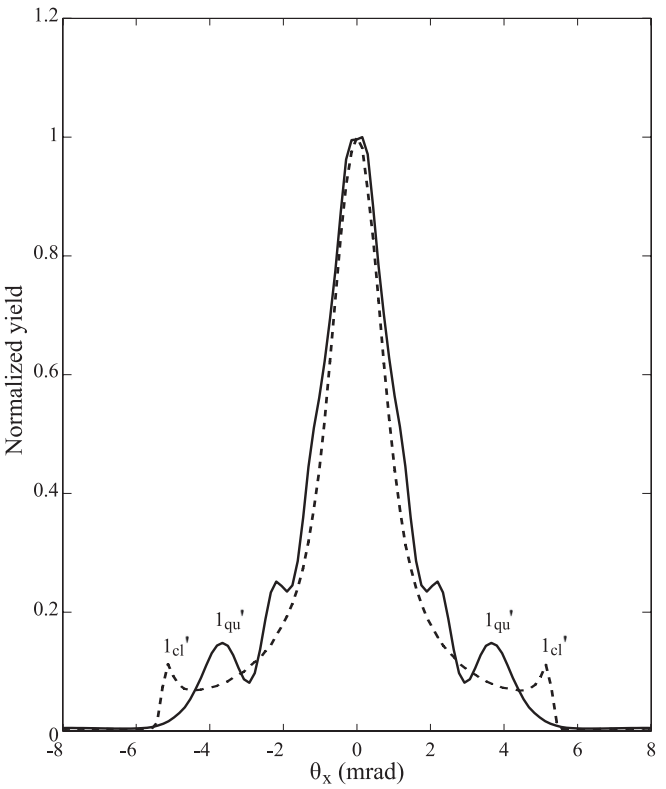

FIG. 7. One-dimensional normalized angular distribution of 1-MeV positrons transmitted through a 200-nm-long (11,9) SWCN represented initially as the ensemble of Gaussian wave packets with $\sigma_\theta = 0.1\theta_c$ (solid line) and the corresponding classical angular distribution (dashed line).

Figure 7 shows the one-dimensional normalized angular distribution of the transmitted positrons for $E = 1$ MeV and $L = 200$ nm with the beam represented initially as the ensemble of Gaussian wave packets with $\sigma_\theta = 0.1\theta_c = 0.73$ mrad, giving $\sigma_\rho = 0.19$ nm, together with the corresponding classical distribution, with the initial beam diverging from the nanotube axis (see Fig. 3). In the case of the quantum distribution, the initial number of positrons is $N = 151$. The quantum distribution is the superposition of a bell-shaped component and a component consisting of three pairs of maxima. The strongest pair of maxima lies at points ± 3.7 mrad and the two weaker pairs of maxima lie at points ± 2.2 and ± 1.2 mrad. These maxima should be explained by the fact that the inverse function of the corresponding angular transmission function is triple valued on the bright side of the classical primary rainbow [see Fig. 1(b)]. However, the spatial standard deviation of the initial wave packets is not sufficiently large to enable the covering of the three branches of the transmission function. Namely, if an initial wave packet covers two branches of the transmission function joining at point $+0.60$ or -0.60 nm, it cannot cover its third branch, lying in the region below -0.60 nm or above $+0.60$ nm, respectively. Hence, these maxima appear due to the constructive interference of the two rays within the wave packets that have the same position in the transmission angle plane [19–21]. The strongest pair of maxima, being close to the pair of classical primary rainbow maxima, designated by $1_{qu}{}'$, belongs to the quantum primary rainbow and the two weaker pairs of maxima belong to the first and second primary supernumerary rainbows [19–21]. A comparison of this distribution with the corresponding distribution obtained with the initial beam represented as the plane wave shows that the two pairs of stronger maxima of the latter distribution, lying at points ± 3.5 and ± 2.2 mrad, can be viewed as the primary rainbow maxima and the first supernumerary primary rainbow maxima. That is why the pair of maxima lying at points ± 3.5 mrad is designated by 1_{qu}.

Figure 8 shows the one-dimensional normalized angular distribution of the transmitted positrons for $E = 1$ MeV and $L = 200$ nm with the beam represented initially as the ensemble of Gaussian wave packets with $\sigma_\theta = 0.2\theta_c = 1.47$ mrad, giving $\sigma_\rho = 0.09$ nm, together with the corresponding classical distribution, with the initial beam diverging from the nanotube axis. In the case of the quantum distribution, the initial number of positrons is $N = 610$. The quantum distribution is the superposition of a bell-shaped component and a component consisting of only two pairs of maxima. The stronger pair of maxima, being close to the pair of classical primary rainbow maxima, designated by $1_{qu}{}'$, belongs to the quantum primary rainbow and the weaker pair of maxima belongs to the first supernumerary primary rainbow. The positions of these pairs of maxima relative to the classical primary rainbow maxima practically coincide with the positions of the corresponding pairs of maxima appearing in the case of $\sigma_\theta = 0.1\theta_c$. One can anticipate that, for a much larger angular standard deviation of

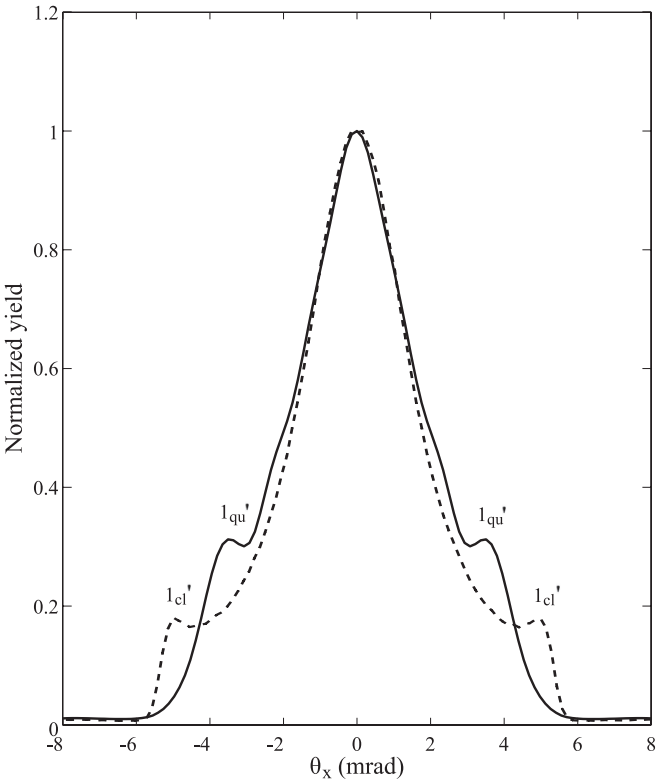

FIG. 8. One-dimensional normalized angular distribution of 1-MeV positrons transmitted through a 200-nm-long (11,9) SWCN represented initially as the ensemble of Gaussian wave packets with $\sigma_\theta = 0.2\theta_c$ (solid line) and the corresponding classical angular distribution (dashed line).

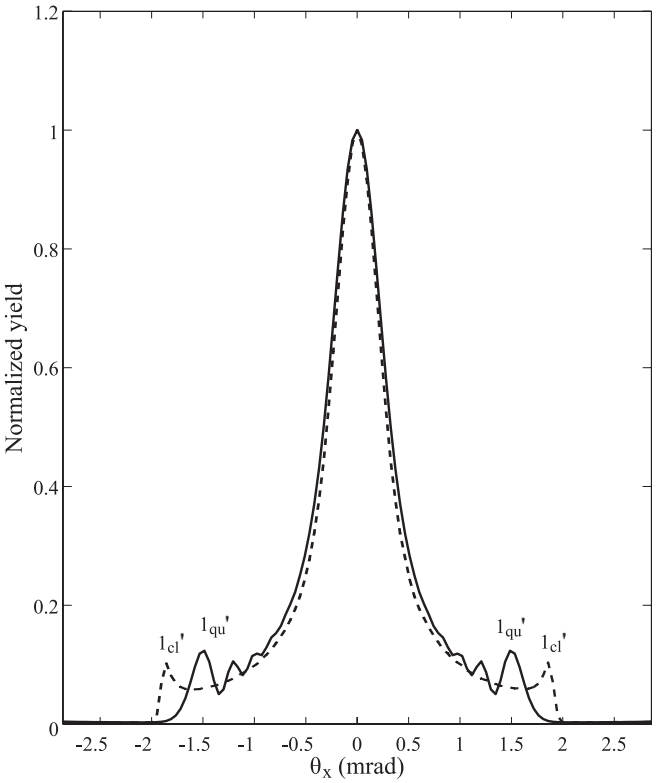

FIG. 9. One-dimensional normalized angular distribution of 10-MeV positrons transmitted through a 560-nm-long (11,9) SWCN represented initially as the ensemble of Gaussian wave packets with $\sigma_\theta = 0.1\theta_c$ (solid line) and the corresponding classical angular distribution (dashed line).

the initial beam, the quantum rainbow maxima will be smeared out as well as the classical rainbow maxima, and the quantum and classical distributions will practically coincide.

Figure 9 shows the one-dimensional normalized angular distribution of the transmitted positrons for $E = 10$ MeV and $L = 560$ nm with the beam represented initially as the ensemble of Gaussian wave packets with $\sigma_\theta = 0.1\theta_c = 0.23$ mrad, giving $\sigma_\rho = 0.08$ nm, together with the corresponding classical distribution, with the initial beam diverging from the nanotube axis. In the case of the quantum distribution, the initial number of positrons is $N = 865$. The quantum distribution is the superposition of a bell-shaped component and a component consisting of four pairs of maxima. The three stronger pairs of maxima lie closer to each other and to the classical primary rainbow maxima than the three pairs of maxima appearing in the case of $E = 1$ MeV. The strongest pair of maxima, being close to the pair of classical primary rainbow maxima, designated by $1_{qu}{}'$, belongs to the quantum primary rainbow and the three weaker pairs of maxima belong to the supernumerary primary rainbows. One can anticipate that, for a much higher positron kinetic energy, the quantum rainbow pattern will contract into a maximum practically coinciding with the classical rainbow maximum.

In our earlier studies of proton channeling in carbon nanotubes, we mentioned the possibility of using the classical angular distributions of transmitted protons, determined by the corresponding rainbow patterns, for exploring the transverse lattice structures of nanotubes [16,29]. Following that idea, we have calculated the angular distribution of 1-MeV positrons transmitted through a 200-nm-long (12,6) SWCN with the beam represented initially as the ensemble of Gaussian wave packets with $\sigma_\theta = 0.1\theta_c = 0.73$ mrad, giving $\sigma_\rho = 0.19$ nm, and compared it with the corresponding above-described distribution obtained with the (11,9) SWCN. The (12,6) SWCN is chiral too. The corresponding distribution has been generated with the initial number of positrons $N = 139$. These distributions are given in Fig. 10. The equilibrium radii of the two nanotubes (R_n) are close to each other—the radius of the former nanotube is 0.63 nm and the radius of the latter one 0.69 nm [13]. In both cases, one circular rainbow line in the transmission angle plane occurs. The radii of these lines ($|\theta_{x1}^{a,1}|$) are close to each other—the radius of the former line is 4.5 mrad and the radius of the latter one 5.3 mrad. This means that it would be difficult to see the difference between the radii of these lines in the classical calculations with the chosen positron beams (with $\sigma_\theta = 0.73$ mrad). However, the quantum calculations show that the distributions obtained with the two nanotubes are considerably different from each other. The former distribution is the superposition of a bell-shaped component and a component consisting of two pairs of maxima while the latter distribution is the superposition of a bell-shaped component and a component consisting of three maxima. Besides, the stronger pair of maxima of the former distribution, designated by $1_{qu}{}'$ for (12,6), is markedly shifted from the strongest pair of maxima of the latter distribution, designated by $1_{qu}{}'$ for (11,9). Consequently, the pronounced

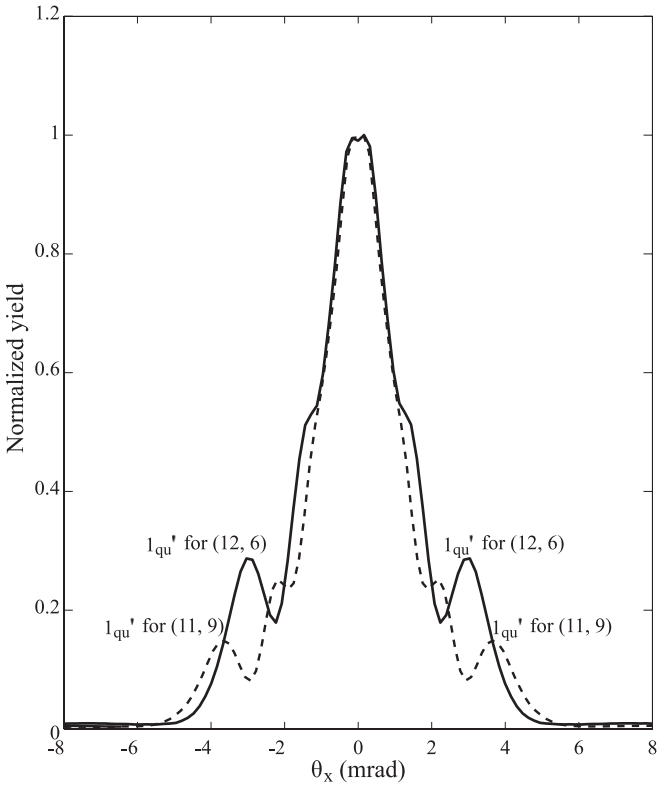

FIG. 10. One-dimensional normalized angular distributions of 1-MeV positrons transmitted through the 200-nm-long (12,6) and (11,9) SWCNs represented initially as the ensemble of Gaussian wave packets with $\sigma_\theta = 0.1\theta_c$ (solid line and dashed line, respectively).

pair of maxima of the former distribution practically coincides with the pair of minima between the two pairs of pronounced maxima of the latter distribution. Therefore, one can state that quantum rainbow channeling could be also applied for the characterization of nanotubes.

IV. CONCLUSIONS

We have investigated the angular distributions of positrons transmitted through the (11,9) SWNC for $E = 1$ MeV and $L = 200$ nm and for $E = 10$ MeV and $L = 560$ nm.

In the case of $E = 1$ MeV and $L = 200$ nm with the positron beam represented initially as the ensemble of Gaussian wave packets with $\sigma_\theta = 0.1\theta_c = 0.73$ mrad, giving $\sigma_\rho = 0.19$ nm, the angular distribution can be viewed as the superposition of a bell-shaped component and a component consisting of three pairs of maxima. These maxima appear due to the constructive interference of two out of three rays within the wave packet that have the same position in the transmission angle plane. The strongest pair of maxima belongs to the quantum primary rainbow and the two weaker pairs of maxima belong to the first and second primary supernumerary rainbows.

When $E = 1$ MeV and $L = 200$ nm with the positron beam represented initially as the ensemble of Gaussian wave packets with $\sigma_\theta = 0.2\theta_c = 1.47$ mrad, giving $\sigma_\rho = 0.09$ nm, the angular distribution is the superposition of a bell-shaped component and a component consisting of only two pairs of maxima. We have concluded that, for a much larger value of σ_θ, the quantum rainbow maxima will be smeared out as well as the classical rainbow maxima, and the quantum and classical distributions will practically coincide.

For $E = 10$ MeV and $L = 560$ nm with the positron beam represented initially as the ensemble of Gaussian wave packets with $\sigma_\theta = 0.1\theta_c = 0.23$ mrad, giving $\sigma_\rho = 0.08$, the angular distribution is the superposition of a bell-shaped component and a component consisting of four pairs of maxima. The three stronger pairs of maxima lie closer to each other and to the classical primary rainbow maxima than the three pairs of maxima appearing for $E = 1$ MeV. It has been concluded that, for a much higher value of E, the quantum rainbow pattern will contract into a maximum practically coinciding with the classical rainbow maximum.

In addition, we have compared the angular distributions of positrons transmitted through the (12,6) and (11,9) SWCNs for $E = 1$ MeV and $L = 200$ nm with the beam represented initially as the ensemble of Gaussian wave packets with $\sigma_\theta = 0.1\theta_c = 0.73$ mrad, giving $\sigma_\rho = 0.19$ nm. The conclusion of the comparison is that quantum rainbow channeling could be employed for the characterization of nanotubes.

ACKNOWLEDGMENT

We acknowledge the support to this work provided by the Ministry of Education, Science, and Technological Development of Serbia through the project *Physics and Chemistry with Ion Beams*, Project No. III 45006.

[1] M. T. Robinson and O. S. Oen, Phys. Rev. **132**, 2385 (1963).
[2] J. Lindhard, K. Dan. Vidensk. Selsk., Mat.-Fys. Medd. **34**, 1, No. 14 (1965).
[3] D. S. Gemmell, Rev. Mod. Phys. **46**, 129 (1974).
[4] N. Nešković, Phys. Rev. B **33**, 6030 (1986).
[5] H. F. Krause, S. Datz, P. F. Dittner, J. Gomez del Campo, P. D. Miller, C. D. Moak, N. Nešković, and P. L. Pepmiller, Phys. Rev. B **33**, 6036 (1986).
[6] S. Petrović, L. Miletić, and N. Nešković, Phys. Rev. B **61**, 184 (2000).
[7] M. Motapothula, S. Petrović, N. Nešković, Z. Y. Dang, M. B. H. Breese, M. A. Rana, and A. Osman, Phys. Rev. B **86**, 205426 (2012).
[8] J. U. Andersen, W. M. Augustyniak, and E. Uggerhøj, Phys. Rev. B **3**, 705 (1971).
[9] M. J. Pedersen, J. U. Anderson, and W. M. Augustyniak, Radiat. Eff. **12**, 47 (1972).
[10] R. Haakenaasen, L. V. Hau, J. A. Golovchenko, J. C. Palathingal, J. P. Peng, P. Asoka-Kumar, and K. G. Lynn, Phys. Rev. Lett. **75**, 1650 (1995).

[11] A. Howie and M. J. Whelan, Proc. R. Soc. London A **263**, 217 (1961).
[12] S. Iijima, Nature (London) **354**, 56 (1991).
[13] R. Saito, G. Dresselhaus, and M. S. Dresselhaus, *Physical Properties of Carbon Nanotubes* (Imperial College Press, London, 1998).
[14] R. H. Baughman, A. A. Zakhidov, and W. A. de Heer, Science **297**, 787 (2002).
[15] V. V. Klimov and V. S. Letokhov, Phys. Lett. A **222**, 424 (1996).
[16] D. Borka, S. Petrović, and N. Nešković, *Channeling of Protons through Carbon Nanotubes* (Nova Science Publishers, New York, 2011).
[17] Z. Zhu, D. Zhu, R. Lu, Z. Xu, W. Zhang, and H. Xia, *Proceedings of the International Conference on Charged and Neutral Particles Channeling Phenomena*, Vol. 5974 (SPIE, Bellingham, WA, 2005), p. 13-1.
[18] G. Chai, H. Heinrich, L. Chow, and T. Schenkel, Appl. Phys. Lett. **91**, 103101 (2007).
[19] H. M. Nussenzveig, *Diffraction Effects in Semiclassical Scattering* (Cambridge University Press, Cambridge, UK, 1992).
[20] J. A. Adam, Phys. Rep. **356**, 229 (2002).
[21] K. W. Ford and J. A. Wheeler, Ann. Phys. **281**, 608 (2002) (reprinted).
[22] F. Michel, G. Reidemeister, and S. Ohkubo, Phys. Rev. Lett. **89**, 152701 (2002).
[23] J. N. L. Connor and D. Farrelly, J. Chem. Phys. **75**, 2831 (1981).
[24] G. Ziegler, M. Rädle, O. Pütz, K. Jung, H. Ehrhardt, and K. Bergmann, Phys. Rev. Lett. **58**, 2642 (1987).
[25] A. W. Kleyn and T. C. M. Horn, Phys. Rep. **199**, 191 (1991).
[26] C. O. Reinhold, J. Burgdorfer, K. Kimura, and M. H. Mannami, Phys. Rev. Lett. **73**, 2508 (1994).
[27] H. Winter and A. Schüller, Prog. Surf. Sci. **169**, 2508 (2011).
[28] S. Miret-Artés and E. Pollak, Surf. Sci. Rep. **67**, 161 (2012).
[29] S. Petrović, D. Borka, and N. Nešković, Eur. Phys. J. B **44**, 41 (2005).
[30] D. Borka, S. Petrović, N. Nešković, D. J. Mowbray, and Z. L. Mišković, Phys. Rev. A **73**, 062902 (2006).
[31] S. Petrović, I. Telečki, D. Borka, and N. Nešković, Phys. Lett. A **372**, 6003 (2008).
[32] G. Molière, Z. Naturforsch. A **2**, 133 (1947).
[33] H. F. Krause, J. H. Barrett, S. Datz, P. F. Dittner, N. L. Jones, J. Gomez del Campo, and C. R. Vane, Phys. Rev. A **49**, 283 (1994).
[34] X. Artru, S. P. Fomin, N. F. Shulga, K. A. Ispirian, and N. K. Zhevago, Phys. Rep. **412**, 89 (2005).
[35] B. R. Appleton, C. Erginsoy, and W. M. Gibson, Phys. Rev. **161**, 330 (1967).
[36] A. Thess, R. Lee, P. Nikolaev, H. Dai, P. Petit, J. Robert, C. Xu, Y. H. Lee, S. G. Kim, A. G. Rinzler, D. T. Colbert, G. Scuseria, D. Tománek, J. E. Fischer, and R. E. Smalley, Science **273**, 483 (1996).
[37] W. H. Press, S. A. Teukolsky, W. T. Vetterling, and B. P. Flannery, *Numerical Recipes in FORTRAN* (Cambridge University Press, Cambridge, UK, 1993).
[38] M. Ćosić, S. Petrović, and N. Nešković (unpublished).